Original Article

JCBFM

Journal of Cerebral Blood Flow & Metabolism
2024, Vol. 44(7) 1145–1162

DOI: 10.1177/0271678X231224508
journals.sagepub.com/home/jcbfm
Sage

The role of serum/glucocorticoid-regulated kinase 1 in brain function following cerebral ischemia

Celeste Yin-Chieh Wu[1,2,*], Yulan Zhang[1,2,*], Li Xu[1,2], Zhihai Huang[1,2], Peibin Zou[1,2], Garrett A Clemons[3], Chun Li[1,2], Cristiane T Citadin[3], Quanguang Zhang[1,2] and Reggie Hui-Chao Lee[1,2]

Abstract

Cardiopulmonary arrest (CA) is a major cause of death/disability in the U.S. with poor prognosis and survival rates. Current therapeutic challenges are physiologically complex because they involve hypoperfusion (decreased cerebral blood flow), neuroinflammation, and mitochondrial dysfunction. We previously discovered novel serum/glucocorticoid-regulated kinase 1 (SGK1) is highly expressed in brain of neurons that are susceptible to ischemia (hippocampus and cortex). We inhibited SGK1 and utilized pharmacological (specific inhibitor, GSK650394) and neuron-specific genetic approaches (shRNA) in rodent models of CA to determine if SGK1 is responsible for hypoperfusion, neuroinflammation, mitochondrial dysfunctional, and neurological deficits after CA. Inhibition of SGK1 alleviated cortical hypoperfusion and neuroinflammation (via Iba1, GFAP, and cytokine array). Treatment with GSK650394 enhanced mitochondrial function (via Seahorse respirometry) in the hippocampus 3 and 7 days after CA. Neuronal injury (via MAP2, dMBP, and Golgi staining) in the hippocampus and cortex was observed 7 days after CA but ameliorated with SGK1-shRNA. Moreover, SGK1 mediated neuronal injury by regulating the Ndrg1-SOX10 axis. Finally, animals subjected to CA exhibited learning/memory, motor, and anxiety deficits after CA, whereas SGK1 inhibition via SGK1-shRNA improved neurocognitive function. The present study suggests the fundamental roles of SGK1 in brain circulation and neuronal survival/death in cerebral ischemia-related diseases.

Keywords

Serum/glucocorticoid-regulated kinase, cerebral ischemia, neuroinflammation, mitochondrial dysfunction, neurological deficits

Received 15 August 2023; Revised 30 November 2023; Accepted 5 December 2023

Introduction

Cardiopulmonary arrest (CA) has a devastating impact on most organ systems due to wide-spread ischemia, frequently leading to death. Only 10% of patients will survive from CA, with major disabilities impacting quality/quantity of life.[1] Most disabilities reflect wide-spread brain neuronal cell death responsible for learning/memory formation (e.g., CA1 region of the hippocampus and cortex). The prevalent quandary in the field of CA is multi-factorial, resulting in whole-body ischemia, which then compromises general circulation and impairs cerebral, renal, and cardiac function. Except for hypothermia,[2] all neuroprotective trials against cerebral ischemia have failed, therefore, new

[1]Stroke Center for Research, Louisiana State University Health, Shreveport, LA, USA
[2]Department of Neurology, Louisiana State University Health, Shreveport, LA, USA
[3]Department of Cellular Biology and Anatomy, Louisiana State University Health, Shreveport, LA, USA

*These authors contributed equally to this work.

Corresponding authors:
Reggie Hui-Chao Lee, Department of Neurology, LSU Health Shreveport, 1501 Kings Hwy, Shreveport, LA 71103-3932, USA.
Email: huichao.lee@lsuhs.edu

Celeste Yin-Chieh Wu, Louisiana State University Health Sciences Center Shreveport, 1501 kings hwy, Shreveport, LA Louisiana 71103, USA.
Email: yinchieh.wu@lsuhs.edu

pharmacological interventions are greatly needed. A major challenge of post-resuscitative care, however, is the highly complicated and multifaceted pathophysiological process of CA, including: 1) hypoperfusion [decreased cerebral blood flow (CBF)]; 2) neuroinflammation; and 3) mitochondrial dysfunction,[3,4] all leading to irreversible neuronal cell death and permanent neurological deficits (e.g., learning/memory and motor impairments). Understanding the pathophysiological mechanism(s) related to CA will lay the foundation for a novel therapy for patients with CA.

Serum/glucocorticoid-regulated kinases (SGKs, members of the serine/threonine-protein kinase family) are expressed in tissues including the heart, liver, pancreas, lung, kidney, intestine, and brain.[5,6] SGKs have been shown to mediate numerous physiological and/or pathophysiological processes, including cell homeostasis and ion transport,[5,7–11] inflammation and oxidative stress,[12,13] and apoptotic/necrotic cell death.[14–17] Activation of SGKs is closely related to heart, liver, and kidney diseases.[5] The impact of SGKs on cerebral ischemia-induced brain injury, however, has rarely been studied and remains to be elucidated. Of the three isoforms of SGKs (SGK1, 2, and 3), we previously demonstrated that CA only enhanced SGK1 mRNA and protein levels in vulnerable brain regions (e.g., hippocampus and cortex).[6]

To elucidate the role of SGK1 in CA-induced brain injury, we utilized specific SGK1 inhibitor (GSK650394) and a cell type-specific genetic approach (adeno-associated virus overexpressing SGK1-shRNA, AAV-SGK1-shRNA) in rat and mouse models of CA such as asphyxial cardiac arrest [CA(rat)] and potassium chloride-induced cardiac arrest [CA(mouse)], respectively.

Materials and methods

Chemicals

Specific SGK1 inhibitor (GSK650394, Tocris, 3572) was dissolved in dimethyl sulfoxide and diluted from a stock solution (1 mM) with sterile water to the desired concentration (1.2 μg/kg).[6] GSK650394 was administered 5 minutes before CA(rat) surgery via intracerebroventricular injection to the third ventricle (2.8 mm posterior to bregma, 0 mm lateral to midline, and 8.3 mm deep). For post-treatment experiments, GSK650394 was delivered directly into the cerebrospinal fluid via intrathecal injection (between the groove of L5 and L6 vertebrae) 30 mins, 1, and 3 days after CA surgery via a 25 μl Hamilton syringe with a 30G 0.5-inch needle.

Animal preparation

All animal experimental procedures were conducted following the Guide for the Care and Use of Laboratory Animals[18] and Animal Research: Reporting of In Vivo Experiments (ARRIVE). All experimental procedures were approved by the Institutional Animal Care and Use Committee at Louisiana State University Health Shreveport. Male Sprague-Dawley rats (270–350 g and 9–10 weeks old) and male C57BL/6 mice (23–27 g) were obtained from Charles River Laboratories. To ensure the present study was performed in an unbiased and rigorous manner, all investigators were blinded to the studies, and all animals were randomized to different treatment groups using Microsoft Excel. It has been well-documented by our group and others that CA causes neuronal cell death mainly in the vulnerable CA1 region of the hippocampus and cortex.[6,19–24] Therefore, we intended to investigate the impact of SGK1 on neuroinflammation, mitochondrial dysfunction, and neuronal cell death in the hippocampus and cortex in the present study.

SGK1 knockdown in the brain by AAV-shRNA

We utilized AAV-PHP.eB expressing SGK1-shRNA and synapsin promoter to knockdown SGK1 gene expression specifically in neurons of C57BL/6 mice. This technology has been well published by our group[25,26] and others.[27–29] The use of human synapsin 1 gene promoter to drive neuron-specific long-term transgene expression in rodents *in vivo* has been validated by Kugler et al.,2003[30] and Jackson et al., 2016.[31] After transduction with AAV, they detected transgene fluorescence exclusively in NeuN-positive cells (neurons) but not in astrocytes or microglia. AAV/PHP.eB-SYN-eGFP-m-SGK1-shRNA mir(3) (AAV-SGK1-shRNA) was obtained from Vector Biolabs (Malvern, PA). The AAV-SGK1-shRNA was diluted in lactated Ringer's solution to a final dose of 1×10^{11} viral particles per mouse. AAV-SGK1-shRNA was administered via retro-orbital injection (100 μl volume). Successful SGK1 knockdown was determined by histological analysis for green fluorescent protein (GFP) signal (Figure 1 (b)), and RT-PCR for SGK1 mRNA levels [Figures 1C (a),(b)] 30 days after viral injection.

Asphyxial cardiac arrest rat model [CA(rat)]

Isoflurane (4%) and a mixture of oxygen and nitrous oxide (30:70) were utilized to anesthetize the animals. After endotracheal intubation, isoflurane was reduced to 1.5% and mechanical ventilation was maintained by VentElite Small Animal Ventilator (Harvard Apparatus, Holliston, MA) at 60 breaths/minute. Two polyethylene catheters (PE-50, Becton Dickinson, Franklin Lakes,

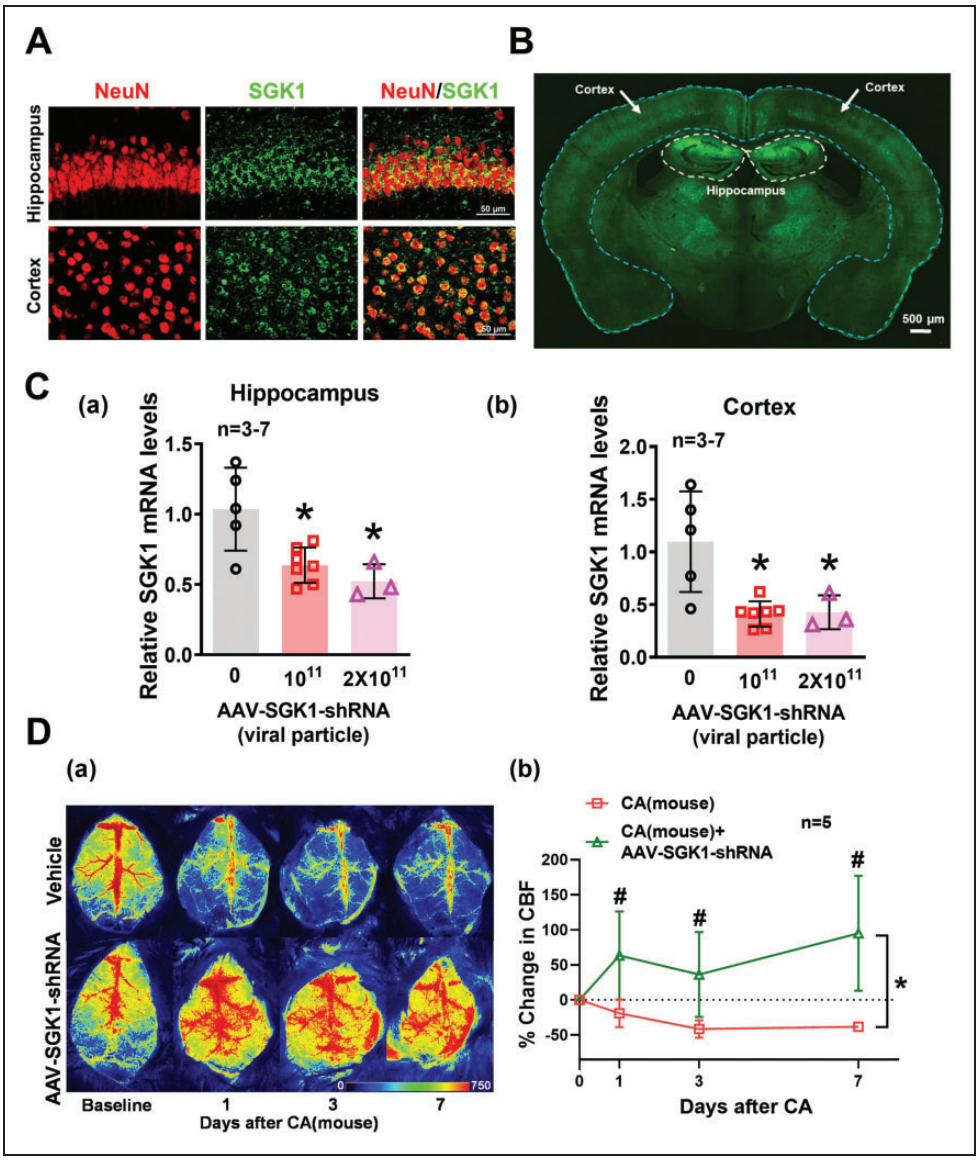

Figure 1. Inhibition of SGK1 (via AAV-SGK1-shRNA) alleviated CA(mouse)-induced hypoperfusion. (A) Representative immunofluorescence images from control mice indicate that co-localization of NeuN (red) and SGK1 (green) in both cortex and hippocampus. Scale bar = 50 μm. (B) Representative images of coronal sections 30 days following virus administration. Scale bar = 500 μm. Green fluorescence indicates GFP-tagged AAV particles. (C) Relative SGK1 mRNA levels in the (a) hippocampus and (b) cortex. Results were expressed as mean ± SD. *$p < 0.05$ indicates significantly different from control mice. (D) (a) Representative flux images of cortical vasculature before (baseline) and 1 day, 3 days, and 7 days after CA. Results were summarized in panel (b). Changes in CBF were presented as percent change from the baseline (CBF 30 min before CA). Results were expressed as mean ± SD. *$p < 0.05$ indicates overall significantly different versus CA-only mice (via two-way ANOVA), #$p < 0.05$ versus respective days after CA.

NJ) were connected to the right femoral vein and artery for drug delivery and blood pressure measurements, respectively. Following femoral vein/artery catheterization, the rats received bolus IV injections of skeletal muscle relaxant (Nimbex, cis-atracurium besylate desolate, 0.27 mg/kg) at 10 minutes interval throughout the surgery. Head and body temperature were maintained at 36.5–37.3 °C by heating pads and lamps. Physiological parameters were monitored and maintained at nominal levels (e.g., pO2: 100 mmHg, pCO2: 35–40 mmHg, blood pressure: 100 mmHg, and pH: 7.4). CA(rat) was induced by blockage of the endotracheal tube using a 1 ml syringe. The ventilator was then turned off and disconnected from the endotracheal tube for 6 minutes to allow complete cerebral anoxia. During cardiopulmonary resuscitation, epinephrine (0.005 mg/kg, intravenous injection) was administered via femoral vein, along with mechanical ventilation using 100% oxygen at a rate of 80 breaths/minute.

Manual chest compression was continuously performed until the mean arterial pressure reached 60 mm Hg. A bolus IV injection of sodium bicarbonate (1 mg/kg, intravenous injection) was then used to reduce respiratory acidosis in the animals. Surgery with similar procedures without asphyxiation was conducted in the control group. The survival rate of rats after CA(rat) was 80%. No significant differences in survival rates were observed between the groups.

Cardiac arrest mouse model [CA(mouse)]

Since there is currently no asphyxial CA mouse model, CA (6 mins) in C57BL/6 mice was induced by injecting KCl via the jugular catheter. Isoflurane (4%) and a mixture of oxygen and air (10:90) were utilized to anesthetize the animals. After endotracheal intubation, isoflurane was reduced to 2% and mechanical ventilation was maintained by VentElite Small Animal Ventilator (Harvard Apparatus, Holliston, MA) at 150 breaths/minute (tidal volume: 200 µl). A polyethylene catheter (PE-10, Becton Dickinson, Franklin Lakes, NJ) was then inserted into the right jugular vein of the mice. Body temperature was maintained at 36.5–37.3 °C by heating pads and lamps, while head temperature was maintained at 37.3–37.7 °C by an objective heater (Warner TC-124, Hamden, CT). Potassium chloride (KCl, 0.5 mEq/mL, 0.05 ml) was administered via jugular vein to induce cardiac arrest, and the ventilator was switched off. 6 minutes after the initial onset of cardiac arrest, ventilator was reconnected to the endotracheal tube, and oxygen was set to 300 ml/minute (air: 0 ml/minute). The respiration rate increased to 200 breaths/minute. Cardiopulmonary resuscitation (300 compressions per minute) was performed using the right index finger until mice showed signs of return of spontaneous circulation. The survival rate after cardiac arrest was 60%, and no differences in survival were observed between groups in this study. The difference between the survival rates of CA(rat) and CA(mouse) is due to the methodologies used to induce ischemia. 6-min asphyxial cardiac arrest is a mild CA rat model as a complete cardiac arrest (heart stops beating) occurs during the last two minutes of apnea. In comparison with asphyxial cardiac arrest rat model, a complete cardiac arrest can be observed immediately after KCl injection in CA mouse model. Both CA animal models have been routinely used in others and our previous studies, yielding similar results with regard to hypoperfusion, neuronal cell death, and neurological deficits.[6,20,32–36] The shRNA experiments were carried out in the mice since they required lower shRNA dosages.

Laser speckle contrast imaging

A longitudinal midline incision was implemented to expose the scalp. Subsequently, the RFLSI III laser imager (RWD) was placed 10 cm above the brain region to record cortical blood flow for 5 mins. Mouse body temperature was maintained at 37 °C.

Reverse transcription real-time polymerase chain reaction

To determine the silencing efficiency of AAV-SGK1-shRNA in the brain, total RNA was extracted from the hippocampus and cortex 30 days after retro-orbital injection of the AAV-SGK1-shRNA. RNA extraction was performed using RNeasy Mini Kit along with the RNase-Free DNase Set (Qiagen, Valencia, California, USA) to eliminate possible contamination of genomic DNA. 0.5 µg of total RNA was then reverse-transcribed into cDNA using the SuperScript™ III First-Strand Synthesis System (Invitrogen, Carlsbad, California, USA). Real-time polymerase chain reaction (20 µl total reaction volume) was carried out with a CFX96TM Touch Real-Time PCR Detection System (Bio-Rad, Hercules, California, USA) in conjunction with the iQ SYBR Green Supermix (Bio-Rad, Hercules, California, USA). The thermal cycle protocol began with an initial denaturation step at 95 °C for 3 minutes, followed by 40 amplification cycles of 95 °C for 10 seconds and 60 °C for 30 seconds. Experiments were performed in triplicate. The relative mRNA levels of SGK1 were calculated utilizing the $2^{-\Delta\Delta Ct}$ formula method. The primer sequences for SGK1 and β-actin were: SGK1: 5′-ATCGTGTTAGCTCCAAAGC-3′, 5′-GTCTGTGATCAGGCATAGC-3′.[37] β-actin: 5′-CCCTAAGGCCAACCGTGAA-3′, 5′-AGAGGCATACAGGGACAACACA-3′.

Stress & toxicity PCR array

RT^2 Profiler™ PCR Array Rat Stress & Toxicity PathwayFinder (330231, Qiagen) was utilized to identify potential signaling pathways involving SGK1-mediated brain injury. 0.5 µg of total RNA was reverse-transcribed into cDNA using RT2 First Strand Kit (Qiagen). Real-time PCR was performed using RT^2 SYBR® Green Mastermixes (Qiagen). The thermal cycle protocol was set as follows: 95 °C for 10 minutes, 40 cycles of 95 °C for 15 seconds and 60 °C for 1 minute. Data analysis was further conducted by Ingenuity Pathway Analysis (IPA, Qiagen).

Bioinformatic analysis

We utilized Qiagen's Ingenuity Pathway Analysis (IPA) software to identify potential diseases and functions

that are most relevant to the array outcomes after CA. Dataset from RT^2 Profiler™ PCR Array and cytokine array was first uploaded to the IPA server. A significant threshold, z-score, was calculated and set to −2 or 2. The core analysis function in the IPA system was used to determine gene networks, canonical pathways, and biological processes. Gene networks and key biological processes were algorithmically generated based on the Ingenuity Pathway Knowledge Base (IPKB).

Measurements of neuroinflammatory cytokines

T-PER™ (ThermoScientific) was utilized for extracting protein from the hippocampus. 40 microglia- and astrocytes-associated neuroinflammatory cytokines from the protein extract (1 μg/μl) were further quantified using the Quantibody® mouse Inflammation Array (QAM-INF-1, RayBiotech), and analyzed using log-log regression curve followed by IPA analysis.

Mitochondrial protein and cytosolic fraction extraction

The mitochondrial protein and cytosolic fraction from the rat hippocampus were extracted by Mitochondria Isolation Kit for Tissue (ThermoScientific). Hippocampal tissue was disrupted in the cold PBS (4 °C) using a tissue grinder. Homogeneous suspension was centrifuged at 1,000 × g for 3 minutes at 4 °C, and the supernatant was discarded. The remaining pellet was incubated in BSA/Reagent A Solution for 2 minutes. Mitochondria Isolation Reagents B and C were added to the pallet in order. The tissue sample was further centrifuged at 3,000 × g for 15 minutes at 4 °C to pellet the mitochondria. After then, the supernatant was collected as cytosolic fractions, while the mitochondrial pellet was lysed with 2% CHAPS in Tris-buffered saline (25 mM Tris, 0.15 M NaCl; pH 7.2).

Capillary-based immunoassay

3 μg of mitochondrial and cytoplasmic protein lysate (1 μg/μl) from the hippocampus were utilized to determine SGK1 protein levels following CA via Wes system (Biotechne) coupled with a 12–230 kDa Separation Module. The primary antibodies used included anti-SGK1 (1:50) (ab32374, Abcam), TOM20 (1:1000) (Cell Signaling, 42406), N-myc downstream regulated gene 1 (Ndrg1) (Cell Signaling, 5196), pNdrg1 (Cell Signaling, 3217), and SRY-box transcription factor 10 (Sox10) (Novus, NBP2-59620). pNdrg1 levels were measured via Stellar NIR Detection Module, while SGK1 protein levels were normalized to the total protein of the sample via Total Protein Detection Module.

Mitochondrial oxygen consumption rate analysis

The mitochondrial oxygen consumption rate (OCR) in the hippocampus was measured using Agilent Seahorse XFe24 Analyzer (Agilent Seahorse Bioscience, Santa Clara, CA, USA). Rodents were euthanized with isoflurane 3 or 7 days after CA surgery for hippocampal slices. Coronal slices (200 μm in thickness) of the hippocampus were sectioned in the ice-cold artificial cerebrospinal fluid (aCSF, 120 mM NaCl, 3.5 mM KCl, 1.3 mM $CaCl_2$, 1 mM $MgCl_2$ hexahydrate, 0.4 mM KH_2PO_4, 5 mM HEPES, 10 mM glucose, 1 mg/ml of bovine serum albumin, pH 7.4) using a Leica VT1000E vibratome (Leica, Wetzlar, Germany). Stainless steel biopsy punch (Sklar Instruments, West Chester, Pennsylvania, USA) were used to acquire hippocampal tissue sections of 1 mm diameter. The tissue sections were transferred into the XF Islet Capture Microplate (101122-100; Agilent Technologies, Santa Clara, California, USA). The Islet Capture Microplate was acclimated at room temperature for 30 minutes, followed by 37 °C for 1 hr. All dilutions of drugs/mitochondrial complex inhibitors were displayed as follows: first injection: aCSF buffer to serve as vehicle control; second injection: oligomycin (20 μg/ml) to inhibit mitochondrial complex V; third injection: carbonyl cyanide 4-(trifluoromethoxy) phenylhydrazone (FCCP, a mitochondrial uncoupler) at 10 mM plus pyruvate (1 mM) to depolarize the mitochondria; fourth injection: antimycin (20 μM) to inhibit complex III. OCR was presented as the average of all hippocampal sections from each rat. Tissue sections with basal respiration lower than 50 pmol/minute or higher than 200 pmol/minute were unhealthy and removed.

Immunofluorescence staining

Transcardial perfusion was performed with phosphate buffered saline for 2 minutes, followed by 4% paraformaldehyde for 5 minutes (50 ml). Following perfusion, the brain samples were collected and immersed in 4% paraformaldehyde for 2 days at 4 °C. The brain samples were further dehydrated with 30% sucrose solution and embedded in Neg-50™ Frozen Section Medium, Epredia™ (Fisher Scientific, Hampton, NH, USA). Two 25 μm coronal brain sections (Bregma −1.655 mm, −2.055 mm, and −2.555 mm) per animal (n = 4, 8 images for each group) were incubated in permeabilization solution containing 0.4% Triton X-100 (T8787, Sigma-Aldrich, St. Louis, MO, USA) at room temperature for 5 hours, followed by blocking with 3% donkey serum for 1 hour at room temperature. Subsequently, the sections were incubated overnight at room temperature with 1:300 primary antibodies in 0.1% Triton X-100. After washing with 0.1% Triton

X-100, brain sections were incubated with 1:500 appropriate fluorescent secondary antibodies (Invitrogen, A11004, A31573, A32931) for 1 hour at room temperature. The following primary antibodies were used in our study: microtubule-associated protein 2 (MAP2, Santa Cruz, sc-74421), myelin basic protein (MBP, Abcam, ab62631), dMBP (Millipore, AB5864), glial fibrillary acidic protein [GFAP, (Millipore, AB5804, for hippocampal tissue) and (Invitrogen, 13-0300, for cortical tissue)], ionized calcium binding adaptor molecule 1 (Iba1, Wako Chemicals, 019-19741), tumor necrosis factor alpha (TNF-α, Proteintech, 60291-1-Ig), SGK1 (Abcam, ab239812), Ndrg1 (Cell signaling technology, 31815S), SOX10 (Proteintech, 10422-1-AP), Oligo 2 (R&D System, AF2418), and neuronal nuclear protein (NeuN, Millipore, ABN91).

Spine density analysis

Golgi Staining was performed according to the manufacturer's instructions (FD NeuroTechnologies, PK401). Briefly, the fresh brain samples were harvested and stored in the impregnation solution at room temperature for two weeks in the dark. Next, the brain samples were immersed in Solution C at room temperature for 72 hours in the dark. Subsequently, the 100 μm coronal sections were sliced by using a Vibrating Microtome (Leica, VT1000E) and mounted on the gelatin-coated slides (PO101, FD NeuroTechnologies). After rinsing with Milli-Q water, the brain sections were stained with a staining solution at room temperature for 10 minutes, followed by rinsing with Milli-Q water. At last, the brain sections were dehydrated by ethanol, cleared in xylene, and then mounted with Permount® mounting medium (SP15-100, Fisher Scientific, Hampton, NH, USA). The images were captured using a Zeiss AxioObserver & Apotome microscope. The Image J software was used to process and analyze images. The spine density was counted from 5 brains per group, 2 sections per brain, and 2 dendrites per image.

T-maze spontaneous alternation test

All mice were handled for 5 minutes in a dimly lit room to acclimate to human handling before CA or sham surgery. The T-maze apparatus was made of white acrylic plates [two goal arms: 25 (L) × 10 (W) × 15 (H) cm, one start arm: 30 (L) × 11 (W) × 15 (H) cm]. Three days after CA/sham surgery, mice were transferred to a dimly lit room for 30 minutes to acclimate to the environment. At the beginning of the trial, mice were placed in the starting area and were allowed to explore the right or left target arm (first run). Once the mouse entered one of the target arms (all four paws of the mouse entered the target arm), the investigators gently blocked the opposite arm. The mice were allowed to stay in the target arm for 30 seconds. Then, the investigator gently placed the mouse back in the starting area again. The mouse was allowed to choose between the left and right goal arms again (second run). Mice underwent 2 trials per day at 20 minutes interval for 3 consecutive days. Each trial consisted of 2 separate runs, with a time limit of 2 minutes per run.

Barnes maze test

The Barnes maze test was performed to evaluate spatial learning and memory in the animals. The apparatus consisted of a circular platform (120 cm in diameter, 0.5 cm in thickness, and 100 cm in height) with 18 equally spaced holes (10 cm in diameter), including a target quadrant with a hidden box located under the escape hole. The test consisted of two stages across 4 days: training trial (days 1–3) and probe test (day 4). During the training trials, the animals were placed in the center of the platform and allowed to explore freely for 3 minutes, with bright lights and intense noise serving as stimuli. In case the animals were unable to locate the hidden box within the stipulated time, the researcher guided the animals to the box and allowed them to stay inside for 30 seconds. The trajectory of the animals was recorded using the overhead camera connected to the ANY-maze video tracking software (Stoelting, Wood Dale, IL, USA). For the probe test, the hidden box was removed on day 4, and the escape hole was blocked. The animals were allowed to explore the platform for 90 seconds. The total time spent by the animals in the target quadrant and the number of target hole entrances were recorded.

Elevated plus maze test

The elevated plus-maze test was used for evaluating anxious-like behaviors. In brief, the apparatus was 50 cm above the floor and consisted of two open arms and two closed arms, arranged in opposite pairs and a central area. The closed arms were surrounded by 50-cm-high walls. The animals were placed in the center of the maze and allowed to explore freely for 5 minutes. The number of open arms entries and the time spent in the open arms were recorded using ANY-maze video tracking software.

The adhesive removal test

The adhesive removal test was employed to measure somatosensory deficits. Two small adhesive strips (0.2 cm × 0.2 cm) were placed on the forepaw of the animals. The time taken to remove the adhesive strips

was recorded. Three consecutive trials were conducted, and the mean time of three trials was analyzed.

The hanging wire test

The hanging wire test was performed to evaluate the forelimb grip strength and motor coordination. A metal wire was extended and hung 50 cm above the ground. The animals were placed on the metal wire and the hanging wire score was recorded, which was determined by a 5-point scale: 0, the animals fall off the wire immediately; 1, the animal hangs on the wire with its front paws; 2, the animal attempts to climb on the wire, with 2 forepaws hanging on the wire; 3, the animal uses one or two hind legs when attempts to grasp the wire using its front paws with one or both hind limbs; 4, the animal grabs the wire with its four paws and wraps its tail around the wire. Three trials were performed for each animal, with 5-minute intervals, and the highest score was recorded and used for statistical analysis.

Statistical analysis

Results were expressed as mean ± standard deviation (SD). Groups were tested for normal distribution using the Shapiro-Wilk test in GraphPad Prism 9. Statistical analysis was evaluated by independent t-test (for GSK650394 post-treatment study, neuropeptide Y ELISA study, and mitochondrial oxygen consumption rate mouse model), two-way ANOVA (for laser speckle contrast imaging, BM, adhesive removal, and hanging wire studies), and one-way ANOVA with Sidak or Tukey's *post-hoc* test as appropriate with GraphPad Prism 9.

Sample size justification

The number of animals per group was determined based on our previous publications[6,19–22,26,38–40] and power analysis with $p < 0.05$ (a power of 0.95) (home page.univie.ac.at/robin.rist/samplesize.php?test = anova). We also adjusted animal numbers based on standard deviation if standard deviation was higher than projected to ensure sufficient power. Per our recent publications, 5 animals per group is sufficient for studies related to cerebral blood flow measurements.[19,20,26,38,39] Animal behavior studies required at least 6 animals per group to achieve statistical power,[6,21,39] while a minimum sample size of 3–4 is required to achieve the desired level of confidence for brain histology, inflammatory arrays, and Seahorse analyzer experiment.[21,22,26,40] As for the Ndrg1/SOX10 study (Figure 5), we compared the overall differences (across 1, 3, and 7 days after cardiac arrest) between cardiac arrest and treatment groups (via two-way ANOVA with Tukey's post-hoc). Therefore, 4 animals per group for each day after cardiac arrest is sufficient to achieve statistical power.[38,41]

Results

Inhibition of SGK1 (via AAV-SGK1-shRNA) alleviated CA(mouse)-induced hypoperfusion

Immunofluorescence staining was first utilized to identify specific cell types that express SGK1 in the hippocampus and cortex. Co-staining of NeuN and SGK1 indicates that SGK1 is mainly located in neurons of the hippocampus and cortex (Figure 1A). We thus used AAV-PHP.eB expressing SGK1-shRNA and synapsin promoter to knockdown SGK1 gene expression specifically in neurons of C57BL/6 mice. Fluorescent images of the coronal section of the brain suggest that AAV-PHP.eB vector system can efficiently deliver genes across the blood-brain barrier 30 days after a single retro-orbital injection of AAV-SGK1-shRNA (Figure 1B). In addition, AAV-SGK1-shRNA reduced SGK1 mRNA levels in the hippocampus (0.64 ± 0.13 and 0.52 ± 0.12 v. 1.04 ± 0.30) and cortex (0.41 ± 0.12 and 0.43 ± 0.16 v. 1.10 ± 0.48) [Figures 1C(a) and (b)]. We further investigated the impact of neuronal SGK1 inhibition on cortical CBF after CA by *in vivo* laser speckle contrast imaging. Cortical hypoperfusion was observed 1, 3 and 7 days after CA [$F(1, 8) = 11.88$, $p = 0.0087$], while inhibition of SGK1 via AAV-SGK1-shRNA counteracted hypoperfusion [Figures 1D(a) and (b)].

Inhibition of SGK1 (via AAV-SGK1-shRNA) alleviated CA-induced neuroinflammation

To identify possible cellular/subcellular signaling pathways that lead to SGK1-mediated brain injury, we screened 84 stress and toxicity related genes in the hippocampus via RNA microarray (Qiagen Stress & Toxicity Pathway Finder) coupled with pathway-focused gene expression analysis (IPA). Interestingly, neuroinflammation is significantly enhanced in rats subjected to CA. [Figures 2A(a) and (b)]. Similar results were further confirmed by an independent approach in mice subjected to CA. Results from histopathological analysis indicates that the number of Ionized calcium binding adaptor molecule 1 (Iba1)+ (hippocampus: 200.80 ± 25.83 v. 100.00 ± 3.90; cortex: 224.30 ± 30.47 v. 101.70 ± 6.40) and tumor necrosis factor alpha (TNF-α)+ microglia (activated microglia) (hippocampus: 175.40 ± 29.78 v. 100.00 ± 7.86; cortex: 194.20 ± 22.48 v. 100.00 ± 6.80) and glial fibrillary acidic protein (GFAP)+ astrocytes (hippocampus: 181.70 ± 6.24 v. 100.00 ± 5.86; cortex: 221.0 ± 13.41 v.

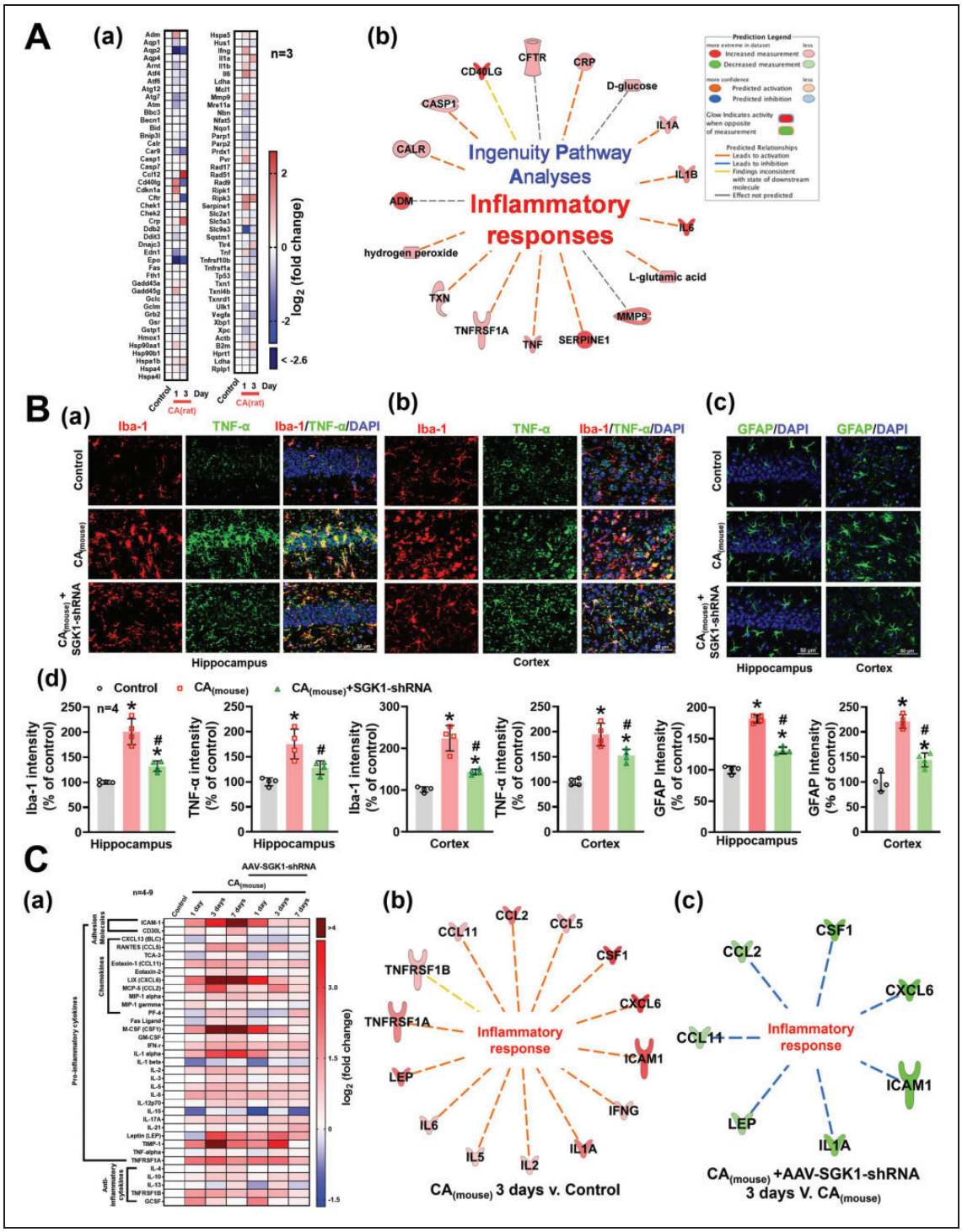

Figure 2. Inhibition of SGK1 (via AAV-SGK1-shRNA) alleviated CA-induced neuroinflammation. (A) Total RNA was extracted from the rat hippocampus 1 and 3 days after CA(rat). mRNA levels of 84 stress and toxicity-related genes in the hippocampus were measured via RT^2 Profiler^{TM} PCR Array. (a) Heatmap of mRNA expression of the selected genes involved in cellular responses to stress and toxic compounds. (b) Results from PCR array were further analyzed by QIAGEN Ingenuity Pathway Analysis. (B) (a, b, c) Representative fluorescence images of Iba-1 (red), TNF-α (green), and GFAP (green) in the mouse hippocampus and cortex 7 days after CA(mouse). Relative immunofluorescence intensity of Iba-1, TNF-α, and GFAP was summarized in panel (d) ($n = 4$). (C) Heatmap of protein levels of the inflammatory cytokines involved in the activation of microglia and astrocytes. (a) Total protein was extracted from mice 1, 3, and 7 days after CA(mouse). Results from inflammatory array were analyzed by QIAGEN Ingenuity Pathway Analysis as shown in panels (b) and (c). Results were expressed as mean $\pm$ SD. $^{*}p < 0.05$ versus control, $^{\#}p < 0.05$ versus respective days after CA.

100.00 ± 17.99) significantly increased in mice subjected to CA [Figures 2B(a) to (d)]. However, treatment with specific SGK1 inhibitors (GSK or AAV-SGK1-shRNA) alleviated microglia activation (Iba1: 132.10 ± 10.38 and 143.70 ± 6.45; TNF-α: 128.40 ± 13.41 and 152.30 ± 12.83) and astrogliosis (131.30 ± 5.21 and 144.10 ± 13.91) [Figures 2B(a) to (d)]. Protein chip assay was further performed to analyze 40 inflammatory cytokines/chemokines in the hippocampus of mice subjected to CA with/without AAV-SGK1-shRNA treatment. Utilizing IPA, results from protein chip assay predicted neuroinflammation was enhanced following CA(mouse). Contrarily, treatment of AAV-SGK1-shRNA drastically reduced inflammatory cytokine levels.

Treatment of specific SGK1 inhibitor, GSK650394, maintained hippocampal mitochondrial function following CA

To determine whether SGK1 contributes to CA-induced mitochondrial dysfunction, we first measured SGK1 protein levels in the mitochondria and cytoplasm of the hippocampus from control and rats subjected to CA. Only rats were utilized in this study to obtain enough hippocampal tissue for protein analysis. Results from capillary-based immunoassay indicated that that the localization of the SGK1 protein notably shifted from the cytoplasm to the mitochondria following CA(rat) (0.015 ± 0.005 v. 0.030 ± 0.013) [Figures 3A(a) and (b)]. To determine if inhibition of SGK1 protects mitochondrial function after CA, tissue sections from coronal slices of the rat hippocampus were further utilized to study mitochondrial stress after CA via Seahorse respirometry. Mitochondrial maximal respiration (70.08 ± 18.66 and 73.60 ± 20.80 v. 113.40 ± 10.69), proton leak-linked respiration (33.57 ± 7.35 and 44.36 ± 8.48 v. 48.30 ± 2.70), and reserve respiratory capacity (8.61 ± 7.85 and -5.60 ± 7.59 v. 28.61 ± 10.05), indicators of the capability of mitochondria to acclimate rising metabolic demands during stress, significantly decreased 3 and 7 days after CA [Figures 3B (a) to (d)] to suggest CA-induced mitochondrial dysfunction. Treatment with GSK650394 improved mitochondrial function leading to better neuronal survival and functional outcomes after CA [Figures 3B(a) to (d)]. Results as shown in Figure 3 were further confirmed using tissue from the mouse model (Supplementary Figure S1). We found similar results from the mouse hippocampal slices as inhibition of SGK1 (via AAV-SGK1-shRNA) promoted basal respiration (127.10 ± 18.07 v. 97.70 ± 16.56), ATP-linked respiration (64.02 ± 7.49 v. 53.66 ± 10.43), Proton leak-linked respiration (47.09 ± 5.00 v. 38.78 ± 5.61), and maximal respiration (123.60 ± 14.87 v. 102.90 ± 15.57) after CA.

Knockdown of SGK1 alleviated dendrisomatic neuronal injury, while preserved dendritic spine density after CA

Due to the prevalence of delayed neuronal cell death occurs 3 to 7 days after CA,[19] brain histopathology was performed 7 days after CA to investigate the neuroprotective effects of SGK1 inhibition on delayed neuronal injury in the CA1 region of the hippocampus and cortex. We analyzed levels of microtubule-associated protein (MAP2) and myelin basic protein complex (MBP) in CA mice treated with/without AAV-SGK1-shRNA. MAP2 and MBP are responsible for cytoskeletal assembly and myelination during neuronal growth, synapse formation, and axon guidance. They have been widely used as a biomarker for early neuronal damage after cerebral ischemia.[42,43] Dendrisomatic neuronal injury (via MAP2) (hippocampus: 79.80 ± 3.30 v. 99.95 ± 3.62; cortex: 75.72 ± 3.03 v. 100.30 ± 3.03) [Figures 4A(a) and (b)], myelin degradation (via degraded myelin basic protein complex, dMBP) (hippocampus: 128.00 ± 9.21 v. 100.10 ± 2.71; cortex: 138.70 ± 7.74 v. 99.22 ± 7.82) [Figures 4B(a) and (b)], and a decrease in dendritic spine density (via Golgi staining) can be observed in the CA1 region of the hippocampus and cortex 7 days after CA(mouse) [Figures 4C(a) to (c)]. Intriguingly, dendrisomatic neuronal injury, demyelination, and the reduction of dendritic spine density in the cortex and hippocampus of the CA mice were significantly reduced by AAV-SGK1-shRNA treatment (Figures 4A to C).

SGK1 regulates Ndrg1/SOX signaling pathway

Previous studies report Ndrg1 is a key downstream substrate for SGK1.[55,56] To identify potential signaling pathways involved in SGK1-mediated neuronal injury. We utilized capillary-based immunoassay to examine whether SGK1 can modulate Ndrg1 after CA. Phosphorylation of Ndrg1 in the hippocampus was increased following CA as compared to control, while inhibition of SGK1 via AAV-shRNA reduced Ndrg1 phosphorylation (Figures 5A(a) and (b)). Further IPA analysis predicts a crucial role of SOX10 in SGK1/Ndrg1 cascade of central nervous system (Figure 5C). We further determined whether SGK1/pNdrg1 regulates SOX10 levels. As shown in Figures 5A(a) and (b) and 5B(a) to (c), there is a negative correlation between pNdrg1 and SOX10 protein levels, while downregulation of SGK1 via AAV-shRNA after CA can reduce pNdrg1 to increase SOX10 levels.

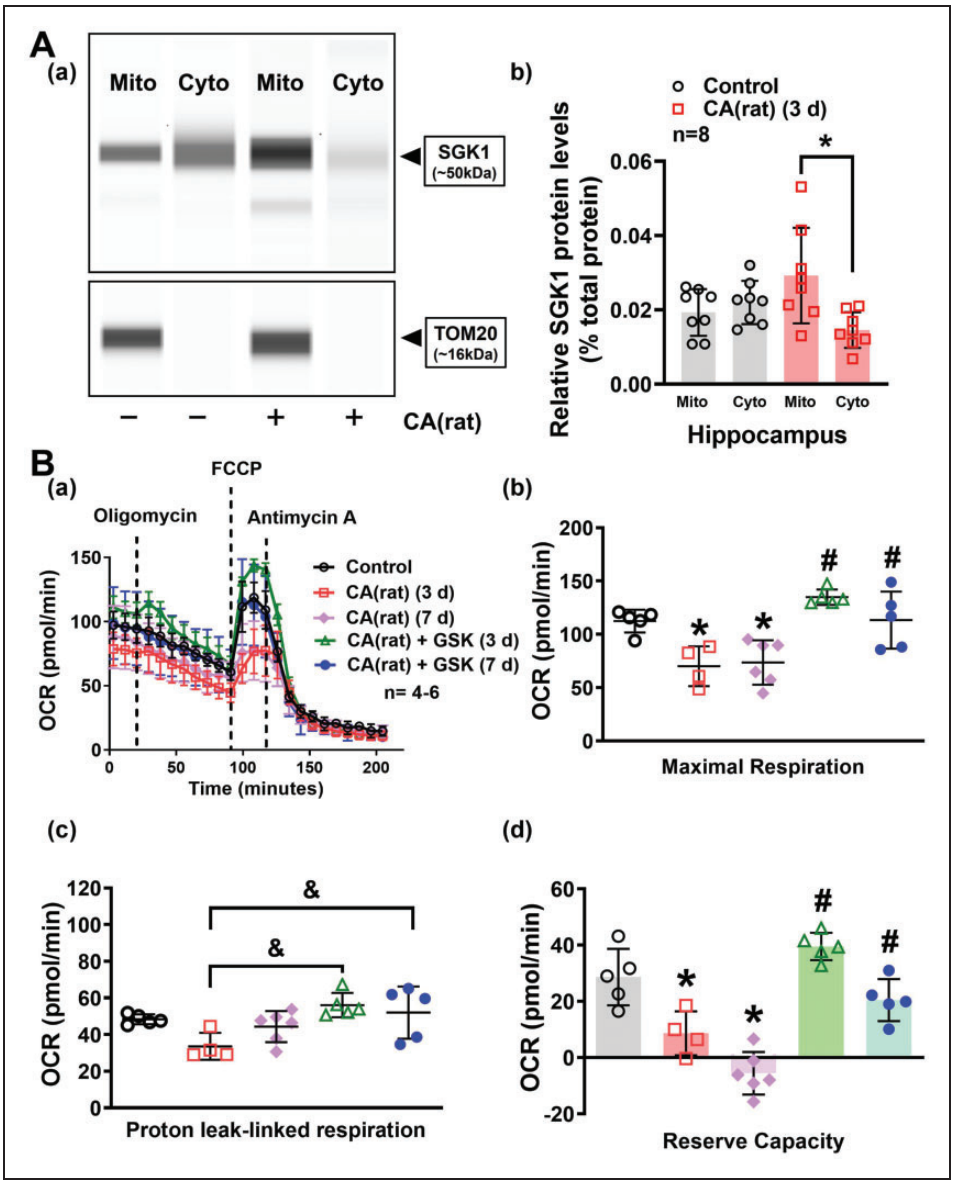

Figure 3. Inhibition of SGK1 (via GSK650394) alleviated CA(rat)-induced mitochondrial dysfunction in the hippocampus. (A) Representative images of the computer-generated pseudo bands from the capillary-based immunoassay. (a) SGK1 and TOM20 band at 50 and 16 kDa, respectively. (b) Hippocampal SGK1 protein levels in the mitochondria (mito) and cytosolic fraction (cyto) in control and rats subjected to CA were normalized to the total protein. Results were expressed as mean ± SD, $^{*}p < 0.05$ as compared to mitochondrial SGK1 protein levels 3 days after CA. (B) (a) Mitochondrial oxygen consumption rate (OCR) was measured in hippocampal slices 3 and 7 days after CA(rat) via a Seahorse XF24 analyzer. Results were summarized in panels (b, c, d). Treatment with GSK650394 (GSK) improved mitochondrial maximal respiration, proton leak-linked respiration, and reverse capacity 3 and 7 days after CA(rat). $^{*}p < 0.05$ versus control, $^{\#}p < 0.05$ versus respective days after CA. $^{\&}p < 0.05$ versus 3 days after CA(rat). All data were expressed as mean ± SD.

SGK1 inhibition reversed CA-induced neurocognitive and motor deficits

Results from T and Barnes mazes suggest that learning and memory impairments in mice subjected to CA surgery were significantly alleviated by AAV-SGK1-shRNA, as demonstrated by a significant increase in alternation ratio (52.78 ± 6.81 v. 27.78 ± 23.57) [Figure 6A(b)] and quadrant occupancy (48.95 ± 15.15 v. 37.54 ± 10.95) [Figure 6B(b)]. Furthermore, mice subjected to CA exhibited less time spent (22.72 ± 20.92 v. 93.37 ± 38.66) and a fewer number of entries (6 ± 3 v. 11 ± 3) in the open arms from the elevated plus maze test as compared with control mice [Figure 6C(b)], which suggests anxiety-related behavior. The anxiety following CA was notably alleviated in CA(mouse)+AAV-SGK1-shRNA group (56.69 ± 52.99

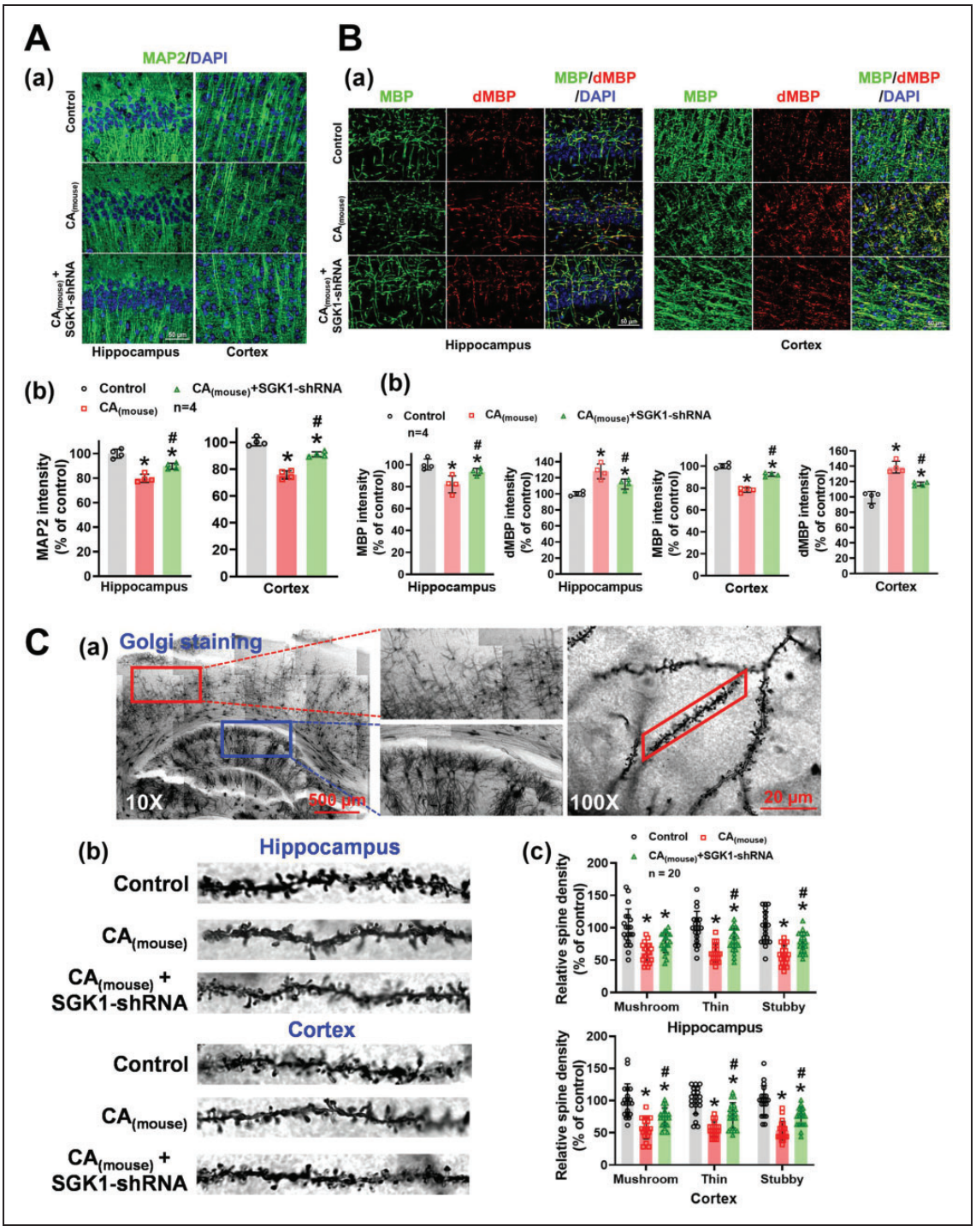

Figure 4. Knockdown of SGK1 alleviated dendrisomatic neuronal injury, while preserving dendritic spine density after CA. (A) (a) Representative immunofluorescence images of MAP2 (green) in the CA1 region of the hippocampus and cortex 7 days after CA (mouse). Quantification of the results were summarized in panel (b). (B) Representative images of MBP (green) and degraded MBP (dMBP, red) staining in the CA1 region of the hippocampal and cortex were shown in (a). Quantification of the relative MBP and dMBP fluorescence intensity was shown in panel (b). (C) (a) Representative images of dendritic spines in the hippocampus (blue rectangle) and cortex (red rectangle) via Golgi staining. (b) Selected dendritic segments in the CA1 region of the hippocampus and cortex from control and mice subjected to CA surgery. The total number of mushroom, thin, and stubby spines was manually counted and summarized in panel (c). All data were expressed as mean ± SD. $^{*}p < 0.05$ versus control, $^{\#}p < 0.05$ versus respective days after CA.

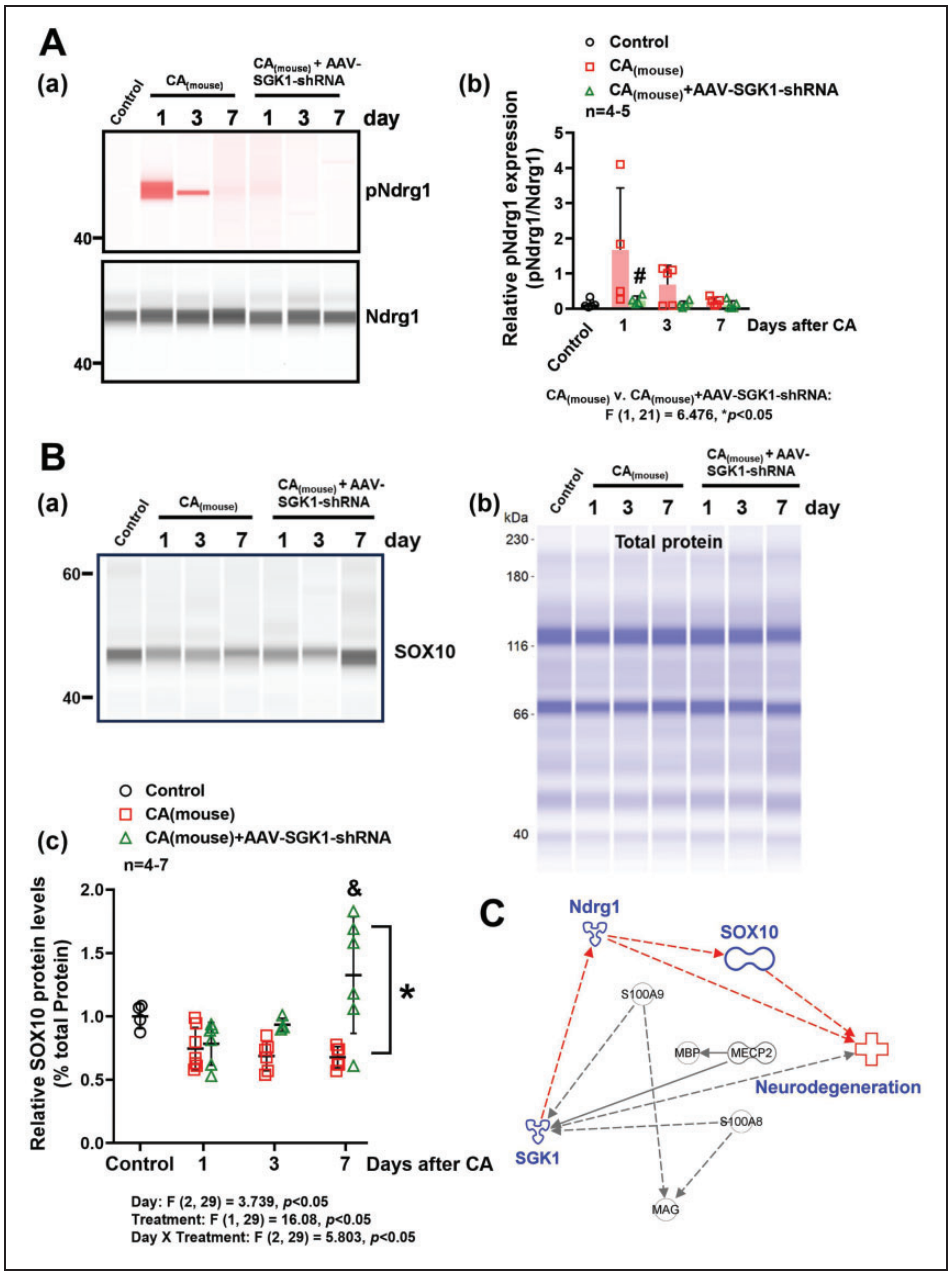

Figure 5. Hippocampal SGK1 levels and Ndrg1 phosphorylation were enhanced concurrently with decreased SOX10 levels after CA, while inhibition of SGK1 via AAV enhanced SOX10 levels. (A, B) Relative protein levels of total Ndrg1, phosphorylated Ndrg1 (pNdrg1), and SOX10 in the hippocampus were measured by capillary-based immunoassay. pNdrg1, total Ndrg1, and SOX10 band at 50, 48, and 55 kDa, respectively. Results were normalized with total Ndrg1 [A (a)] or total protein [B (b)] (for SOX10) and summarized in panels A (b) and B (c). $^{*}p < 0.05$ versus CA only group evaluated by two-way ANOVA with Tukey's post-hoc. $^{\#}p < 0.05$ versus 1 day after CA. $^{\&}p < 0.05$ versus CA only group (1, 3, 7 days) and CA+AAV-SGK1-shRNA group (1 day). (C) Ingenuity Pathway Analyses indicates SGK1 can phosphorylate Ndrg1 to modulate SOX10.

and 9 ± 4). The hanging wire and adhesive removal tests were also performed to assess the impact of SGK1 inhibition on motor function. As shown in Figures 6D and E, mice subjected to CA had lower hanging wire score [$F(1, 26) = 62.42$, $p < 0.0001$] and spent drastically more time [$F(1, 46) = 89.81$, $p < 0.0001$] to remove adhesives as compared with control mice, while motor deficits were mitigated with AAV-SGK1-shRNA.

Discussion

CBF derangements often occur after CA, which are highlighted by prolonged hypoperfusion that lasts

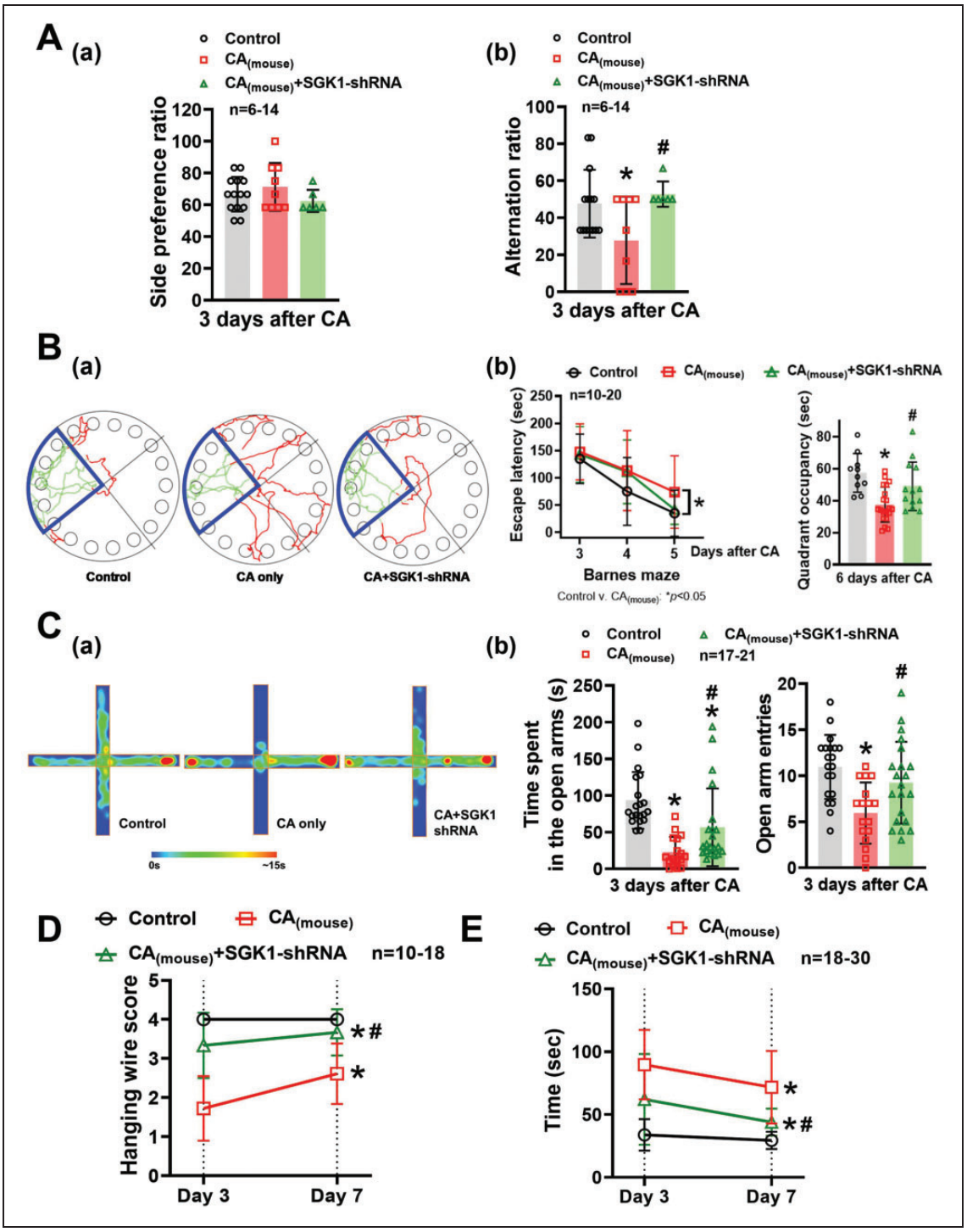

Figure 6. SGK1 inhibition reversed CA-induced cognitive and motor deficits. (A) 3 days after CA, the mice were subjected to T-maze spontaneous alternation test for assessment of functional learning/memory. Results from T-maze test were summarized in panels (a, side preference ratio) and (b, alternation ratio). (B) Barnes maze was utilized to evaluate mouse's long-term memory 3–6 days after CA. (a) Representative tracking plots of control, CA(mouse), and CA(mouse)+SGK1-shRNA groups during the last training day (day 6 after CA). (b) The escape latency to find the target box on days 3, 4, and 5 after CA, and the quadrant occupancy on day 6 after CA. (C) Anxiety-like behavior in mice 3 days after CA was evaluated by elevated plus-maze. The degree of anxiety was determined by the time spent and number of entries in the open arms. (a) Representative heat maps of the elevated plus-maze test from the control, CA only, and CA+SGK1-shRNA groups. Time spent in the open arms and the number of open arm entries were summarized in panel (b). Mouse's motor function 3 and 7 days after CA was studied via hanging wire test (D) and adhesive removal test (E). Data were expressed as mean ± SD. $^{*}p < 0.05$ versus control, $^{\#}p < 0.05$ versus CA only.

from hours to days following the initial onset of CA. The consequence of hypoperfusion leads to neuronal cell death and eventual neurocognitive (learning/memory) deficits after ischemia.[3,4,19,20] Hence, alleviation of post-resuscitative hypoperfusion will provide beneficial neurological outcomes after ischemia for days.[19,20] Mechanisms underlying SGK1-mediated hypoperfusion remain unknown. We previously discovered hypoperfusion following rat model of CA is driven by excessive activation of the sympathetic nervous system,[19] which results in massive vasoconstrictors released [e.g., neuropeptide Y (NPY)] impairing brain circulation.[21] Whether SGK1 causes this elevation in NPY after CA was further investigated in the present study. Results from ELISA indicate that SGK1 inhibition via GSK650394 can reduce NPY levels after CA (Supplementary Figure S2). According to our prior study,[21] inhibition of neuropeptide Y via peptide YY $(PYY)_{3–36}$ can counteract hypoperfusion[21] providing neuroprotection similar to attenuation of SGK1 via GSK650394 or AAV-SGK1-shRNA. These results suggest that SGK1 inhibition indirectly modulates CBF through modifying the expression/levels of NPY. Further studies are needed to elucidate whether the alterations in NPY levels after CA are due to changes in NPY release or NPY synthesis.

In addition to hypoperfusion, cerebral ischemia results in anaerobic metabolism, which produces metabolic/toxic waste (e.g., lactate and reactive oxygen species) to activate inflammatory responses.[44–50] SGKs has been reported to regulate various inflammatory and oxidative stress mediators (e.g., nuclear factor κB, nitric oxide, interleukins, P38 mitogen-activated protein kinases, reactive oxygen species).[14–17] These results were further supported by our Qiagen's Stress & Toxicity PCR array, IPA analysis, and immunofluorescence staining, which suggests a possible pro-inflammatory role of SGK1 in the brain following CA.

Mechanisms underlying SGK1-mediated neuroinflammation following cerebral ischemia remains unknown. We have demonstrated in the present study via protein chip assay and IPA that 7 proinflammatory cytokines [e.g., CCL2, CCL11, Leptin (LEP), IL-1α, ICAM-1, CXCL6, and CSF-1] were significantly enhanced following CA but attenuated by AAV-SGK1-shRNA. Importantly, prior research suggests SGK1 activation promotes astrocyte-derived CCL2 and IL-1 levels,[51–53] which is essential for the recruitment of various immune cells including microglia.

Apart from hypoperfusion and neuroinflammation, proper maintenance of mitochondrial function (via generation of ATP) is imperative for neuronal survival in CA. From the present study, we have discovered that distribution of SGK1 protein significantly shifted from the cytoplasm to mitochondria following CA. The subcellular location of SGK1 with respect to neurodegenerative diseases (e.g., cerebral ischemia) is unknown. The majority of the studies suggest that SGK1 is mainly located in the cytoplasm.[54,55] However, the subcellular localization of SGK1 can be further controlled by cell cycle and various stress stimuli. For example, SGK1 was discovered to be present in the nucleus of rat mammary epithelial tumors,[56,57] while SGK1 is enriched in the mitochondria under osmotic stress and oxidation–reduction (Redox) conditions.[54,58]

We also established that inhibition of SGK1 can improve mitochondria's capability to adapt to CA-induced cellular stress in both CA rat and mouse models. To our knowledge, we are the first to investigate the detrimental impact of SGK1 on mitochondrial dysfunction after cerebral ischemia. Mitochondrial Ca^{2+} overload in the brain can alter mitochondrial membrane permeability, ATP production, and ultimately lead to mitochondrial dysfunction.[59,60] Whether SGK1 controls mitochondrial Ca^{2+} homeostasis after CA is an attractive avenue to follow as prior studies indicate that SGKs controls various ion channels including Na/Cl symporter, Na^+, Ca^{2+}, and K^+ channels.[5,7–11]

It remains largely unknown about the signaling axis of SGK1 causing neuronal damage. We have demonstrated that SGK1 can phosphorylate N-myc downstream regulated gene 1 after CA (Figures 5A(a) and (b)). Although the critical role of Ndrg1 in neurodegenerative diseases is unclear, phosphorylation of Ndrg2 on Ser350 has been reported to promote neuronal cell death via caspase-3-mediated pathway.[61] Further Ingenuity Pathways Analysis (IPA) of Ndrg1 predicts potential signaling pathway of SOX10 in neurodegenerative diseases. SOX10 is a key transcription factor, which controls signal transduction between the mitochondria and nucleus.[62] Furthermore, SOX10 is responsible for proliferation, migration, survival, and differentiation of various neuronal cells,[63,64] while deletion of SOX10 leads to neuronal cell death.[63] In the present study, we have established this novel SGK1/Ndrg1/SOX10 axis using capillary-based immunoassay as attenuation of SGK1 and Ndrg1 phosphorylation leads to an increase in SOX10 expression and more favorable neuronal survival and functional outcomes.

As shown in Figures 4, cytoskeletal deficits and the loss of dendritic spines in both the CA1 region of the hippocampus and cortex are a key indication of cognitive decline after CA. We utilized the T maze, Barnes maze, and elevated plus maze to study whether SGK1 inhibition via AAV protects learning/memory and anxiety-related behavior after CA. The importance of studying anxiety is that CA survivors often suffer from anxiety, which leads to recurrent cardiac arrest and

premature death.[65] We observed alleviation of learning/memory and anxiety deficits by inhibition of SGK1 via AAV-SGK1-shRNA in CA-treated mice, which indicates that targeting SGK1 is a potential therapeutic.

Although the FDA has approved the first drug specifically for ICV injection (Brineura, for Batten disease), as well as two AAV-based gene therapies, Luxturna (for Leber congenital amaurosis) and Zolgensma (for spinal muscular atrophy),[66,67] we are aware that ICV injection of GSK650394 or AAV-SGK1-shRNA treatment may not be a viable option for patients who suffer from CA. We have developed an alternative route of drug administration (via intrathecal injection) to deliver GSK650394 directly into cerebrospinal fluid. This injection is minimally invasive with short recovery time. In this pilot study, post-treatment of GSK650394 in the mice provides robust learning/memory improvement, similar to ICV injection of GSK650394 or AAV-SGK1-shRNA treatment (Supplementary Figure S3).

Limitations of the study

To date, most cardiac arrest rodent models have only been considered in male rodents because continual variance of female hormones [e.g., 17β-estradiol (E_2)] can have an influence over the drug/treatment, rendering it difficult to dissect and analyze function or mechanism. It is well-documented that females are less susceptible to post-ischemic brain damage in humans as well as in experimental models of ischemia.[68,69] Therefore, we did not include female animals in the present study.

Due to technical difficulties, we were not able to directly study the impact of Ndrg1/SOX10 pathway on SGK1-mediated functional outcomes after cardiac arrest. There are currently no commercially available specific inhibitors and knockout mouse-line targeting Ndrg1 or SOX10. In fact, SOX10-deficient mice are not viable.[70] Additionally, knockdown of two genes (e.g., SGK1/Ndrg1 or SGK1/SOX10) simultaneously via AAV is challenging due to the capacity of the plasmid and subsequent cloning. To study SGK1's interaction with Ndrg1 and SOX10 after cardiac arrest, we performed co-immunofluorescence staining for 1) Sox10 with neuronal marker (NeuN) and 2) Ndrg1 with neuronal, oligodendrocyte, and myelin markers [NeuN, Olig2, and myelin basic protein (MBP), respectively]. From our observations, Sox10 is predominantly localized within neurons (Supplementary figure S4A), while Ndrg1 is heavily concentrated in the oligodendrocytes and myelin sheaths (Supplementary figure S4B). The crosstalk between neurons and oligodendrocytes in the central nervous system has received increasing attention over the past decade. This is because neurons provide signals to promote myelin formation and repair.[71–73] Contrarily, oligodendrocytes deliver essential nutrients to neurons, which is essential for axon maturation and orientation.[71–73] These bidirectional interactions are crucial for proper nervous system function repair.[71–73] Disruption of the reciprocal signaling relationship between neurons and oligodendrocytes can lead to several neurodegenerative diseases (e.g., Alzheimer's disease, multiple sclerosis, Parkinson's disease, and stroke).[73–75] Further studies are needed to elucidate the involvement of the Ndrg1/SOX pathway in SGK1 inhibition-induced outcomes.

Conclusion

We have established in the present study that upregulation of SGK1 in the brain after CA is detrimental, whereas the use of GSK650394 or AAV-SGK1-shRNA to inhibit SGK1 can alleviate CA-induced hypoperfusion, neuroinflammation, mitochondrial dysfunction, and neuronal injury resulting in better neurocognitive outcomes. We have also demonstrated that SGK1 mediates neuronal injury by regulating the Ndrg1-SOX10 axis. Since the FDA has approved over 46 kinase-related drugs for the treatment of various diseases, the present work can revolutionize how we implement resuscitation protocols in the near future.

Funding

The author(s) declared the following potential conflicts of interest with respect to the research, authorship, and/or publication of this article: NIH/NINDS 5R01NS126273-02 and the AHA 23TPA1069224, 21CDA856826, 19CDA34660032.

Declaration of conflicting interests

The author(s) declared no potential conflicts of interest with respect to the research, authorship, and/or publication of this article.

Authors' contributions

Celeste Y. Wu conducted protein analyses, including hippocampal protein extraction, capillary-based immunoassay, and protein array analysis. Dr. Wu also contributed to the preparation of this manuscript.

Yulan Zhang conducted hippocampal protein extraction, capillary-based immunoassay, histological slide preparation, and animal behavioral analyses. Ms. Zhang also contributed to the preparation of this manuscript and experiment planning.

Li Xu assisted with the protein extraction, mitochondrial function, and protein analyses.

Zhihai Huang assisted with the behavioral and brain histological studies.

Peibin Zou performed histological analysis, as well as animal perfusion,

Garrett A. Clemons assisted with studies related to neuroinflammation.
Chun Li assisted with the behavioral and brain histological studies.
Cristiane T. Citadin provided technical support relating to RNA extraction and real-time PCR.
Quanguang Zhang provided scientific input and direction to the present research.
Reggie H. Lee directed the present research as well as performed CA surgeries, CBF measurements, and behavioral studies. Dr. Lee also aided in the draft of the manuscript.

ORCID iD

Reggie Hui-Chao Lee https://orcid.org/0000-0001-6099-8333

Supplementary material

Supplemental material for this article is available online.

References

1. Virani SS, Alonso A, Aparicio HJ, et al. Heart disease and stroke statistics-2021 update: a report from the American heart association. *Circulation* 2021; 143: e254–e743.
2. Neumar RW, Nolan JP, Adrie C, et al. Post-cardiac arrest syndrome: epidemiology, pathophysiology, treatment, and prognostication. A consensus statement from the international liaison committee on resuscitation (American Heart Association, Australian and New Zealand Council on Resuscitation, European Resuscitation Council, Heart and Stroke Foundation of Canada, InterAmerican Heart Foundation, Resuscitation Council of Asia, and the Resuscitation Council of Southern Africa); the American Heart Association Emergency Cardiovascular Care Committee; the Council on Cardiovascular Surgery and Anesthesia; the Council on Cardiopulmonary, Perioperative, and Critical Care; the Council on Clinical Cardiology; and the Stroke Council. *Circulation* 2008; 118: 2452–2483.
3. Harukuni I and Bhardwaj A. Mechanisms of brain injury after global cerebral ischemia. *Neurol Clin* 2006; 24: 1–21.
4. Sabri M, Lass E and Macdonald RL. Early brain injury: a common mechanism in subarachnoid hemorrhage and global cerebral ischemia. *Stroke Res Treat* 2013; 2013: 394036.
5. Lang F, Bohmer C, Palmada M, et al. (Patho)physiological significance of the serum- and glucocorticoid-inducible kinase isoforms. *Physiol Rev* 2006; 86: 1151–1178.
6. Lee RH, Grames MS, Wu CY, et al. Upregulation of serum and glucocorticoid-regulated kinase 1 exacerbates brain injury and neurological deficits after cardiac arrest. *Am J Physiol Heart Circ Physiol* 2020; 319: H1044–H1050.
7. Bohmer C, Palmada M, Kenngott C, et al. Regulation of the epithelial calcium channel TRPV6 by the serum and glucocorticoid-inducible kinase isoforms SGK1 and SGK3. *FEBS Lett* 2007; 581: 5586–5590.
8. Lang F, Henke G, Embark HM, et al. Regulation of channels by the serum and glucocorticoid-inducible kinase – implications for transport, excitability and cell proliferation. *Cell Physiol Biochem* 2003; 13: 41–50.
9. Grahammer F, Artunc F, Sandulache D, et al. Renal function of gene-targeted mice lacking both SGK1 and SGK3. *Am J Physiol Regul Integr Comp Physiol* 2006; 290: R945–950.
10. Artunc F, Ebrahim A, Siraskar B, et al. Responses to diuretic treatment in gene-targeted mice lacking serum- and glucocorticoid-inducible kinase 1. *Kidney Blood Press Res* 2009; 32: 119–127.
11. Helms MN, Yu L, Malik B, et al. Role of SGK1 in nitric oxide inhibition of ENaC in Na+-transporting epithelia. *Am J Physiol Cell Physiol* 2005; 289: C717–726.
12. Alliston TN, Gonzalez-Robayna IJ, Buse P, et al. Expression and localization of serum/glucocorticoid-induced kinase in the rat ovary: relation to follicular growth and differentiation. *Endocrinology* 2000; 141: 385–395.
13. Avishai-Eliner S, Yi SJ and Baram TZ. Developmental profile of messenger RNA for the corticotropin-releasing hormone receptor in the rat limbic system. *Brain Res Dev Brain Res* 1996; 91: 159–163.
14. Baban B, Liu JY and Mozaffari MS. SGK-1 regulates inflammation and cell death in the ischemic-reperfused heart: pressure-related effects. *Am J Hypertens* 2014; 27: 846–856.
15. BelAiba RS, Djordjevic T, Bonello S, et al. The serum- and glucocorticoid-inducible kinase sgk-1 is involved in pulmonary vascular remodeling: role in redox-sensitive regulation of tissue factor by thrombin. *Circ Res* 2006; 98: 828–836.
16. Eylenstein A, Schmidt S, Gu S, et al. Transcription factor NF-kappaB regulates expression of pore-forming Ca2+ channel unit, Orai1, and its activator, STIM1, to control Ca2+ entry and affect cellular functions. *J Biol Chem* 2012; 287: 2719–2730.
17. Rusai K, Prokai A, Szebeni B, et al. Gender differences in serum and glucocorticoid regulated kinase-1 (SGK-1) expression during renal ischemia/reperfusion injury. *Cell Physiol Biochem* 2011; 27: 727–738.
18. *Guide for the Care and Use of Laboratory Animals*. 8th ed. Washington, DC: The National Academies Press, 2011.
19. Lee RH, Couto ESA, Lerner FM, et al. Interruption of perivascular sympathetic nerves of cerebral arteries offers neuroprotection against ischemia. *Am J Physiol Heart Circ Physiol* 2017; 312: H182–H188.
20. Lee RH, Couto ESA, Possoit HE, et al. Palmitic acid methyl ester is a novel neuroprotective agent against cardiac arrest. *Prostaglandins Leukot Essent Fatty Acids* 2019; 147: 6–14.
21. Lee RH, Wu CY, Citadin CT, et al. Activation of neuropeptide Y2 receptor can inhibit global cerebral Ischemia-Induced brain injury. *Neuromolecular Med* 2022; 24: 97–112.
22. Wu CY, Couto ESA, Citadin CT, et al. Palmitic acid methyl ester inhibits cardiac arrest-induced neuroinflammation and mitochondrial dysfunction. *Prostaglandins Leukot Essent Fatty Acids* 2020; 165: 102227.

23. Neumann JT, Cohan CH, Dave KR, et al. Global cerebral ischemia: synaptic and cognitive dysfunction. *Curr Drug Targets* 2013; 14: 20–35.
24. Dave KR, Anthony Defazio R, Raval AP, et al. Protein kinase C epsilon activation delays neuronal depolarization during cardiac arrest in the euthermic arctic ground squirrel. *J Neurochem* 2009; 110: 1170–1179.
25. Couto ESA, Wu CY, Clemons GA, et al. Protein arginine methyltransferase 8 modulates mitochondrial bioenergetics and neuroinflammation after hypoxic stress. *J Neurochem* 2021; 159: 742–761.
26. Acosta CH, Clemons GA, Citadin CT, et al. PRMT7 can prevent neurovascular uncoupling, blood-brain barrier permeability, and mitochondrial dysfunction in repetitive and mild traumatic brain injury. *Exp Neurol* 2023; 366: 114445.
27. Blizard S, Park D, O'Toole N, et al. Neuron-Specific IMP2 overexpression by synapsin Promoter-Driven AAV9: a tool to study its role in axon regeneration. *Cells* 2021; 10: 2654.
28. Finneran DJ, Njoku IP, Flores-Pazarin D, et al. Toward development of neuron specific transduction after systemic delivery of viral vectors. *Front Neurol* 2021; 12: 685802.
29. McLean JR, Smith GA, Rocha EM, et al. Widespread neuron-specific transgene expression in brain and spinal cord following synapsin promoter-driven AAV9 neonatal intracerebroventricular injection. *Neurosci Lett* 2014; 576: 73–78.
30. Kugler S, Kilic E and Bahr M. Human synapsin 1 gene promoter confers highly neuron-specific long-term transgene expression from an adenoviral vector in the adult rat brain depending on the transduced area. *Gene Ther* 2003; 10: 337–347.
31. Jackson KL, Dayton RD, Deverman BE, et al. Better targeting, better efficiency for wide-scale neuronal transduction with the synapsin promoter and AAV-PHP.B. *Front Mol Neurosci* 2016; 9: 116.
32. Hutchens MP, Traystman RJ, Fujiyoshi T, et al. Normothermic cardiac arrest and cardiopulmonary resuscitation: a mouse model of ischemia-reperfusion injury. *Journal of Visualized Experiments: JoVE* 2011; 54: 3116.
33. Grace PM, Shimizu K, Strand KA, et al. (+)-naltrexone is neuroprotective and promotes alternative activation in the mouse hippocampus after cardiac arrest/cardiopulmonary resuscitation. *Brain Behav Immun* 2015; 48: 115–122.
34. Wu CYC, Lerner FM, Couto ESA, et al. Utilizing the modified T-maze to assess functional memory outcomes after cardiac arrest. *J Visual Exp: JoVE* 2018; 131: 56694.
35. Cohan CH, Neumann JT, Dave KR, et al. Effect of cardiac arrest on cognitive impairment and hippocampal plasticity in Middle-aged rats. *PloS One* 2015; 10: e0124918.
36. Quillinan N, Deng G, Shimizu K, et al. Long-term depression in Purkinje neurons is persistently impaired following cardiac arrest and cardiopulmonary resuscitation in mice. *J Cereb Blood Flow Metab* 2017; 37: 3053–3064.
37. Doyle MA, Stark AR, Fejes-Toth G, et al. Behavioral effects of SGK1 knockout in VTA and dopamine neurons. *Sci Rep* 2020; 10: 14751.
38. Clemons GA, Silva ACE, Acosta CH, et al. Protein arginine methyltransferase 4 modulates nitric oxide synthase uncoupling and cerebral blood flow in Alzheimer's disease. *J Cell Physiol* 2022. DOI: 10.1002/jcp.30858.
39. Wu CYC, Lopez-Toledano MA, Daak AA, et al. SC411 treatment can enhance survival in a mouse model of sickle cell disease. *Prostaglandins Leukot Essent Fatty Acids* 2020; 158: 102110.
40. Yang L, Wu C, Li Y, et al. Long-term exercise pretraining attenuates Alzheimer's disease-related pathology in a transgenic rat model of Alzheimer's disease. *Geroscience* 2022; 44: 1457–1477.
41. Acosta CH, Clemons GA, Citadin CT, et al. A role for protein arginine methyltransferase 7 in repetitive and mild traumatic brain injury. *Neurochem Int* 2023; 166: 105524.
42. Mages B, Fuhs T, Aleithe S, et al. The cytoskeletal elements MAP2 and NF-L show substantial alterations in different stroke models while elevated serum levels highlight especially MAP2 as a sensitive biomarker in stroke patients. *Mol Neurobiol* 2021; 58: 4051–4069.
43. Zhan X, Cox C, Ander BP, et al. Inflammation combined with ischemia produces myelin injury and Plaque-Like aggregates of myelin, amyloid-beta and AbetaPP in adult rat brain. *J Alzheimers Dis* 2015; 46: 507–523.
44. Fowler JH, McQueen J, Holland PR, et al. Dimethyl fumarate improves white matter function following severe hypoperfusion: involvement of microglia/macrophages and inflammatory mediators. *J Cereb Blood Flow Metab* 2018; 38: 1354–1370.
45. Back DB, Kwon KJ, Choi DH, et al. Chronic cerebral hypoperfusion induces post-stroke dementia following acute ischemic stroke in rats. *J Neuroinflammation* 2017; 14: 216.
46. Wakita H, Tomimoto H, Akiguchi I, et al. A cyclooxygenase-2 inhibitor attenuates white matter damage in chronic cerebral ischemia. *Neuroreport* 1999; 10: 1461–1465.
47. Lee KM, Bang J, Kim BY, et al. Fructus mume alleviates chronic cerebral hypoperfusion-induced white matter and hippocampal damage via inhibition of inflammation and downregulation of TLR4 and p38 MAPK signaling. *BMC Complement Altern Med* 2015; 15: 125.
48. Zlokovic BV. Neurovascular mechanisms of Alzheimer's neurodegeneration. *Trends Neurosci* 2005; 28: 202–208.
49. Nishio K, Ihara M, Yamasaki N, et al. A mouse model characterizing features of vascular dementia with hippocampal atrophy. *Stroke* 2010; 41: 1278–1284.
50. Yamada M, Ihara M, Okamoto Y, et al. The influence of chronic cerebral hypoperfusion on cognitive function and amyloid beta metabolism in APP overexpressing mice. *PloS One* 2011; 6: e16567.
51. Bapat A, Li G, Xiao L, et al. Genetic inhibition of serum glucocorticoid kinase 1 prevents obesity-related atrial fibrillation. *JCI Insight* 2022; 7: e160885.

52. Huang W, Cheng C, Shan WS, et al. Knockdown of SGK1 alleviates the IL-1beta-induced chondrocyte anabolic and catabolic imbalance by activating FoxO1-mediated autophagy in human chondrocytes. *Febs J* 2020; 287: 94–107.
53. Xi X, Zhang J, Wang J, et al. SGK1 mediates hypoxic pulmonary hypertension through promoting macrophage infiltration and activation. *Anal Cell Pathol (Amst)* 2019; 2019: 3013765.
54. Cordas E, Naray-Fejes-Toth A and Fejes-Toth G. Subcellular location of serum- and glucocorticoid-induced kinase-1 in renal and mammary epithelial cells. *Am J Physiol Cell Physiol* 2007; 292: C1971–1981.
55. Alvarez de la Rosa D, Coric T, Todorovic N, et al. Distribution and regulation of expression of serum- and glucocorticoid-induced kinase-1 in the rat kidney. *J Physiol* 2003; 551: 455–466.
56. Maiyar AC, Leong ML and Firestone GL. Importin-alpha mediates the regulated nuclear targeting of serum- and glucocorticoid-inducible protein kinase (sgk) by recognition of a nuclear localization signal in the kinase central domain. *Mol Biol Cell* 2003; 14: 1221–1239.
57. Park J, Leong ML, Buse P, et al. Serum and glucocorticoid-inducible kinase (SGK) is a target of the PI 3-kinase-stimulated signaling pathway. *Embo J* 1999; 18: 3024–3033.
58. Li Y, Liu C, Rolling L, et al. ROS signaling-induced mitochondrial Sgk1 expression regulates epithelial cell renewal. *Proc Natl Acad Sci U S A* 2023; 120: e2216310120.
59. Peng TI and Jou MJ. Oxidative stress caused by mitochondrial calcium overload. *Ann N Y Acad Sci* 2010; 1201: 183–188.
60. Celsi F, Pizzo P, Brini M, et al. Mitochondria, calcium and cell death: a deadly triad in neurodegeneration. *Biochim Biophys Acta* 2009; 1787: 335–344.
61. Kim N, Chen D, Zhou XZ, et al. Death-associated protein kinase 1 phosphorylation in neuronal cell death and neurodegenerative disease. *Int J Mol Sci* 2019; 20: 3131.
62. Mou Z, Tapper AR and Gardner PD. The armadillo repeat-containing protein, ARMCX3, physically and functionally interacts with the developmental regulatory factor Sox10. *J Biol Chem* 2009; 284: 13629–13640.
63. Lai X, Liu J, Zou Z, et al. SOX10 ablation severely impairs the generation of postmigratory neural crest from human pluripotent stem cells. *Cell Death Dis* 2021; 12: 814.
64. Finzsch M, Stolt CC, Lommes P, et al. Sox9 and Sox10 influence survival and migration of oligodendrocyte precursors in the spinal cord by regulating PDGF receptor alpha expression. *Development* 2008; 135: 637–646.
65. Lee J, Cho Y, Oh J, et al. Analysis of anxiety or depression and long-term mortality among survivors of out-of-Hospital cardiac arrest. *JAMA Netw Open* 2023; 6: e237809.
66. FDA, www.fda.gov/news-events/press-announcements/fda-approves-first-treatment-form-batten-disease, https://www.fda.gov/news-events/press-announcements/fda-approves-first-treatment-form-batten-disease (2017, accessed 27 April 2017).
67. Keeler AM and Flotte TR. Recombinant adeno-associated virus gene therapy in light of luxturna (and zolgensma and glybera): where are we, and how did we get here? *Annu Rev Virol* 2019; 6: 601–621.
68. Alkayed NJ, Harukuni I, Kimes AS, et al. Gender-linked brain injury in experimental stroke. *Stroke* 1998; 29: 159–165; discussion 166.
69. Murphy S, McCullough L, Littleton-Kearney M, et al. Estrogen and selective estrogen receptor modulators: neuroprotection in the women's health initiative era. *Endocrine* 2003; 21: 17–26.
70. Truch K, Arter J, Turnescu T, et al. Analysis of the human SOX10 mutation Q377X in mice and its implications for genotype-phenotype correlation in SOX10-related human disease. *Hum Mol Genet* 2018; 27: 1078–1092.
71. Mazuir E, Fricker D and Sol-Foulon N. Neuron-oligodendrocyte communication in myelination of cortical GABAergic cells. *Life (Basel)* 2021; 11: 216.
72. Pantazou V, Roux T, Oliveira Moreira V, et al. Interaction between neurons and the oligodendroglial lineage in multiple sclerosis and its preclinical models. *Life (Basel)* 2021; 11: 231.
73. Duncan GJ, Simkins TJ and Emery B. Neuron-oligodendrocyte interactions in the structure and integrity of axons. *Front Cell Dev Biol* 2021; 9: 653101.
74. Zhang X, Zhang R, Nisa Awan MU, et al. The mechanism and function of glia in Parkinson's disease. *Front Cell Neurosci* 2022; 16: 903469.
75. Zhang R, Chopp M and Zhang ZG. Oligodendrogenesis after cerebral ischemia. *Front Cell Neurosci* 2013; 7: 201.